PCCP

Accepted Manuscript

ROYAL SOCIETY OF CHEMISTRY

www.rsc.org/pccp

Journal Name

ARTICLE

Electrodeposition of gold nanoparticles on aryl diazonium monolayer functionalized HOPG surfaces

Received 00th January 20xx,
Accepted 00th January 20xx

DOI: 10.1039/x0xx00000x

www.rsc.org/

M. C. R. González,[a] A. G. Orive,[a] R. C. Salvarezza [b] and A. H. Creus *[a]

Gold nanoparticles electrodeposition on a modified HOPG surface with a monolayer organic film based on aryl diazonium chemistry has been studied. This organic monolayer is electrochemically grown with the use of 2,2-diphenyl-1-picrylhydrazyl (DPPH), a radical scavenger. The electrodeposition of gold on this modified surface results highly favored resulting in a AuNPs surface density comparable to that found on glassy carbon. AuNPs grow only in the areas covered by the organic monolayer leaving free clean HOPG zones. A progressive mechanism for the nucleation and growth is followed giving AuNPs hemispherical shaped, homogeneously distributed on the surface and of sizes that can be well controlled by the electrodeposition applied potential. By using AFM, C-AFM and electrochemical measurements with the aid of two redox probes, namely $Fe(CN)_6^{4-}$/ $Fe(CN)_6^{3-}$ and dopamine, relevant results about the electrochemical modified surface as well as the gold nanoparticles electrodeposited on them are obtained.

1. Introduction

Electrodeposition is one of the most suitable techniques to form metallic nanoparticles supported on conducting materials.[1, 2] This preparation method has many advantages particularly in the control on the distribution, shape and size of the nanoparticles.[3] In addition, the possibility of forming metallic nanoparticles directly on the substrate surface ensures good electrical connection with the substrate and prevents changes in the nanoparticles reactivity which can take place due to the use of the stabilizers needed in others synthesis methods.[4, 5]

On the other hand, highly oriented pyrolytic graphite (HOPG) is of great interest due to its relation with currently highly used carbon materials as graphene or carbon nanotubes. Moreover, HOPG has large atomically flat areas that make this surface really useful to study changes on the surface by using scanning probes microscopies, in special, Atomic Force Microscopy (AFM) and Scanning Tunneling Microscopy (STM). HOPG basal plane has been shown to be an useful surface in different studies on metallic nanoparticle growth by electrodeposition like shape dependence with the applied potential, adatom surface diffusion, influence of adsorbates, dendritic growth and testing nucleation and growth models.[6-14] Although HOPG basal plane offers and excellent surface to carry out studies through SPMs it has at the same time some limitations particularly important for metallic electrodeposition. First of all, it should be taken into account that electrochemical reactions like metallic electrodeposition on HOPG can result importantly affected if it occurs on the edges of the HOPG electrode itself instead of only on the basal plane.[15] In addition, HOPG is a highly inert chemically surface. For instance, gold and palladium electrodeposition on HOPG results in a very interesting potential-dependent growth mechanisms ranging from nanodisc to dendritic structures but with a poor adherence.[6-9] Thus, the adsorption of most of the metallic particles electrodeposited on HOPG is characterized by a weak interaction between the particle and the surface. Accordingly the resulting electrodes are of a very limited usage. In this way, improvements in the reactivity of the HOPG surface are necessary to obtain a suitable substrate containing electrodeposited metallic nanoparticles.

One of the most promising strategies to change the low chemical reactivity of the HOPG basal plane is based on the use of aryl diazonium salts trying to modify and functionalize at the same time the surface.[16] This method presents numerous advantages, namely it is experimentally easy to implement, can be carried out at room temperature and can be applied at a great variety of surfaces including metals, semiconductors, non-conductive and carbon materials.[17] Modified-surfaces obtained by this process have been important to the development of a large number of applications ranging from nanoelectronics to sensors fields.[18-20] These applications include the ability of these layers to incorporate and

[a] Área de Química Física, Departamento de Química, Facultad de Ciencias, Universidad de La Laguna, Instituto de Materiales y Nanotecnología, Avda. Francisco Sánchez s/n, 38071-La Laguna, Tenerife, Spain.
[b] Instituto de Investigaciones Fisicoquímicas Teóricas y Aplicadas (INIFTA), Facultad de Ciencias Exactas, Universidad Nacional de La Plata - CONICET- Sucursal 4 Casilla de Correo 16, (1900) La Plata, Argentina.

Electronic Supplementary Information (ESI) available: Figure S1 AFM images for multilayer films; Figure S2 AFM image after scratching the NO2-M modified surface; Figure S3 shows AFM image of the NO2-m growth; Figure S4 C-AFM images for NO_2-M; Figure S5 current-potential response in C-AFM on free and modified HOPG surfaces; Figure S6 electrochemical response for multilayer films; Figure S7 Au NPs data obtained at different potentials; Figure S8 Fitting of the results to Sharifker-Hills model; Figure S9 peak to peak potential separation for the different surfaces. See DOI: 10.1039/x0xx00000x

stabilize nanoparticles synthetized ex-situ[21, 22] or directly generated on the substrate by electrochemical[23, 24] or chemical reduction.[25, 26] It is known that the high reactivity of the aryl radicals in solution produces organic films in a very efficient process.[27] However, this efficiency is at the same time and from the electrochemical point of view a great disadvantage due to the generation of a polyaryl layer by radical attack on the grafted molecules that finally produces a thick non-conductive organic multilayer. To obtain films of a lower thickness (including monolayers and sub-monolayers) different approximations have been proposed elsewhere, in special the use of ionic liquids,[28] bulky protecting groups[29] and radical scavengers.[30] Within this last alternative to achieve a good control of the number of layers in the organic film structure, is remarkable the use of 2,2-diphenyl-1-pycrilhidrazyl (DPPH) as a very effective molecule to limit the film growth, giving rise to organic layers of less than 1 nm thickness.[31] One of the main consequence of this thin layers is that its electrical conductivity is not inhibited. Given these recent advances in controlling the properties of producing low thickness films with good charge-transfer properties, our main objective is to use this new knowledge for the electrodeposition of metallic nanoparticles on aryl-modified HOPG substrate. It should be noted that this strategy to control the thickness of the film has been carried out on substrates like GC and PPF but not on HOPG to best of our knowledge. Thus, a profound characterization study of theses systems seems to be needed.

In this work, the study of the gold electrodeposition on modified HOPG surface with an organic monolayer is carried out. The most relevant result is that after the modification of the HOPG surface with a submonolayer of aryl diazonium based organic film, the resultant surface becomes a suitable electrode on which the nucleation and growth of electrodeposited gold nanoparticles (AuNPs) is highly favored. Furthermore, AuNPs grow only in the areas covered by the organic monolayer leaving free clean HOPG zones. In addition, AuNPs nucleation follows a progressive mechanism and are hemispherical shaped, homogeneously distributed on the surface and their sizes can be well controlled with the electrodeposition applied potential. In the present study different aryl diazonium layers are used depending on the principal functional group and the number of layers in its structure. Thus, four cases are studied, namely multilayers (M) and monolayers (m) rich in both, initial -NO_2 and final reduced -NH_2 groups (here on, NO_2-M, NH_2-M, NO_2-m, NH_2-m; capital letters for multilayer). It should be noted that most of the information related with multilayers films will be commented in the Supplementary Information. By using AFM, C-AFM, XPS and electrochemical measurements with the aid of two redox probes, $Fe(CN)_6^{4-}$/ $Fe(CN)_6^{3-}$ and dopamine, relevant results about the electrochemical modified surface as well as the gold nanoparticles electrodeposited on them are obtained. Two main aspects are discussed in this paper: the formation and characterization of organic films on HOPG and secondly the study of the electrodeposition of gold on these modified surfaces.

2. Experimental section

2.1. Materials

HOPG samples (Grade SPI-2) were obtained from SPI Supplies. 4-Nitrobenzenediazonium tetrafluoroborate (NBD), (Aldrich, 97%), Tetrabutylammonium tetrafluoroborate (TBAFB4), (Aldrich, 99%), 2,2-Diphenyl-1-picrylhydrazyl (DPPH) (Sigma-Aldrich), Tetrachloroauric(III) acid, (Aldrich, 99.9%), Sodium Hydroxide (Merck, 99%), Acetonitrile anhydrous (ACN), (Aldrich, 99.8%), Tin(II) chloride, (Aldrich, 98%), Potassium ferrocyanide (Merck), Potassium ferricyanide (Merck) and Dopamine Hydrochloride (Sigma-Aldrich) were used as received.

2.2. Electrochemistry measurements and Surface Modification.

All electrochemical measurements were performed using an Eco Chemie Autolab PGSTAT302 potentiostat/galvanostat. A fresh HOPG surface was prepared using adhesive tape. Special care was taken to avoid as much as possible the effect of surface contamination after the surface cleavage. For electrochemical modification, electrochemical runs were made in a specially designed Teflon-made cell that leaves an exposed working electrode area of 0.20 cm^2, thus eliminating the contribution of the HOPG edges in the voltammograms. A saturated calomel electrode (SCE) and a large area platinum foil were used as reference and counter electrode respectively. All potentials in the text are referred to the SCE scale. Films with a multilayer structure were synthetized from a 10 mM NBD / 0.1 M $TBABF_4$ solution in acetonitrile by three cycles of the working electrode potential from 0.4 to -0.4 V (v= 0.1 V s^{-1}) and fixing at -0.25 V during 300 s. Monolayer organic films were obtained electrochemically in a 1 mM NBD / 0.1 M $TBABF_4$ solution in acetonitrile in the presence of 2mM of DPPH with eight consecutive cycles between 0.5 and -0.6 V (v= 0.1 V s^{-1}). After modification, HOPG samples were sonicated in acetonitrile, thoroughly rinsed with Milli-Q water and finally dried with a stream of nitrogen. Finally, in both cases, monolayer and multilayer organic films, all -NO_2 groups on the surface were totally reduced to -NH_2. For the multilayer case a chemical reduction treating the surface with 1 mM $SnCl_2$ in 0.1M HCl at 80ºC during 2 hours was used. Reduction for the monolayer was made by electrochemical cycling the potential between 0.2 and -1.3 V in H_2O/EtOH 90:10 mixture in the presence of 0.1 M KCl (v=0.05 V s^{-1}). To check the blocking properties of the modified electrodes, the electrochemical response of the $[Fe(CN)_6]^{4-}$/$[Fe(CN)_6]^{3-}$ redox couple as well as dopamine were used. An aqueous solution of 1 mM $K_4[Fe(CN_6)]$/$K_3[Fe(CN)_6]$ in 0.1 M KNO_3 was employed. In this case, cyclic voltammetry was performed by scanning the potential from –0.2 to 0.8 V at 0.01 V s^{-1}. Electrochemical behavior of dopamine was study using a 1 mM dopamine aqueous solution in 0.01M H_2SO_4. In this case, cyclic voltammetry was performed by scanning the potential from 0 to 0.8 V at 0.05 V s^{-1}.

2.3. Characterization of modified surfaces by AFM and C-AFM.

AFM images were obtained in Tapping and Peak-Force mode using a Multimode microscope with a Nanoscope V control unit from Bruker at a scan rate of 0.5–1.2 Hz. To this end, RTESP (271–311

kHz, and 40–80 N m^{-1}) and ScanAsyst-Air-HR (130-160 kHz, and 0.4-0.6 N m^{-1}) tips (from Bruker) were used.

Conductive AFM (C-AFM) measurements were made in contact mode using conductive Pt/Ir coated tips (SCM-PIC, 10-16 kHz, and 0.1–0.4 N m^{-1}, from Bruker). By using C-AFM, topographic features are recorded at the same time that a controlled DC potential is applied between the sample and the tip and the corresponding electrical conductivity distribution image is registered. The current sensitivity was set on 1 nA/V and a bias DC voltage ranging between -1 and 1 V was applied.

2.4. XPS measurements.

High-resolution XPS spectra were collected on an ESCALAB 250 spectrometer equipped with dual aluminum-magnesium anodes, using a monochromatized Al Kα X-ray radiation (hv=1486.6 eV) with a spot size of 650 µm. The spectrometer energy calibration was performed using the Au 4f7/2 and Cu 2p3/2 photoelectron lines. The spectra were collected in constant analyzer energy (CAE) mode with a pass energy of 20 eV and with an energy resolution of about 0.1 eV. For all the measurements, pressure in the ultra high vacuum analysis chamber was less than $9x10^{-9}$ mbar, avoiding that the ejected photoelectrons interact with gas molecules.

3. Results and discussion

3.1. Organic Films Formation.

The cyclic voltammograms recorded on HOPG for NO_2-M formation is shown in Figure 1a. A cathodic irreversible wave can be observed at 0.08 V only in the first potential scan related with the irreversible reduction of NBD on the surface. In successive scans (red and blue lines) there is not contribution in the faradaic current and the peak related with the aryl groups reduction disappears.[32, 33] This fact indicates a complete blocking of the electrode surface by the formation of a compact organic layer since the first cycle.

Figure 1b corresponds to the formation of NO_2-m. In this case, 2 mM of DPPH is added to generate a film with the lowest possible thickness. The first cycle shows a characteristic peak at 0.4 V corresponding to the NBD reduction that in successive cycles disappears. At 0.2 V a peak related with the reduction of DPPH superimposed on that of NBD can be observed. In the positive going direction of the potential, the voltammogram shows the presence of two more signals at 0.14 V and 0.3 V associated with the oxidation reaction of DPPH. [30, 31]

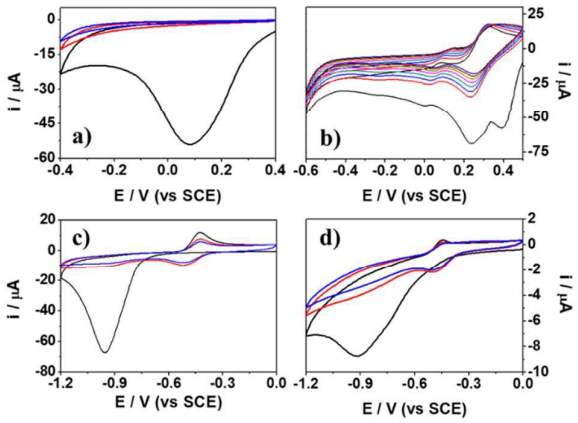

Figure 1. (a) Three consecutive cyclic voltammograms (black, 1st; red, 2nd; blue, 3rd) of HOPG in 10 mM NBD + 0.1 M $TBABF_4$ in acetonitrile (v = 0.1 V s^{-1}); (b) Eight consecutive cyclic voltammograms of HOPG in 1 mM NBD + 0.1 M TBABF4 with 2 mM DPPH in acetonitrile (v = 0.1 V s^{-1}); (c) Three firsts cyclic voltammograms recorded in 0.1 M NaOH of a modified HOPG electrode corresponding to 1a (v = 0.05 V s^{-1}); (d) Three firsts cyclic voltammograms recorded in 0.1 M NaOH of a modified HOPG electrode corresponding to 1b (v = 0.05 V s^{-1}).

To obtain the electrochemical response and the estimation of the HOPG surface coverage, cyclic voltammograms from 0 V to -1.2 V (v = 0.05 V s^{-1}) in 0.1 M NaOH were recorded (Figures 1c-d).[34] The first scan (black line) shows the massive reduction of -NO_2 groups to -NHOH (a four-electron reaction) and to -NH_2 (a six-electron reaction) with an irreversible cathodic wave at -0.95 V (without DPPH, Fig 1c) and -0.9 V (with DPPH, Fig 1d). Repetitive cycles (red and blue lines) implies the disappearance of this last peak while a redox couple related with the system NHOH/NO is observed at -0.4 V. The estimated coverage results in $(13.2 \pm 2.8)*10^{-10}$ mol cm^{-2} for NO_2-M (Fig 1c) and $(2.8 \pm 1.2)*10^{-10}$ cm^{-2}, near a monolayer ($2.4 * 10^{-10}$ mol cm^{-2}),[33] for NO_2-m (Fig 1d). It should be taken into account that these data cannot be used as an estimation of the number of layers of the film because they only corresponds to the response of the electroactive -NO_2 groups, not to the totality of these species on the surface.

Finally, in both cases, for NO_2-M and NO_2-m, all groups on the surface are totally reduced to -NH_2. This step of reduction until amine is necessary to assure that the charge implied in the gold electrodeposition does not result affected by any other reduction reaction. There are many strategies to carry out this final reduction to amine but we have chosen two different methods depending on the structure of the sample. First of all, for NO_2-M, a chemical reduction[25] is selected because this strategy has two principal advantages, on the one hand the reduction promoted by the Sn^{2+} ions occurs not only in the surface but in the inner part of the organic film, on the other hand, surface pinholes generation due to the applied potential[35] is avoided. In the case of NO_2-m reduction to –NH_2 was made electrochemically.[36] In both cases, the almost

complete disappearance of the redox couple located in -0.4 V (not shown) is a good electrochemical test to ensure the reduction of the original $–NO_2$ groups to $–NH_2$.

3.2. XPS, AFM and electrochemical characterization of the organic films.

N1s signal is of interest to determine changes in the oxidation state of nitrogen atoms in the film structure. The chemical nature corresponding to the transformation from the initially $-NO_2$ to the final $-NH_2$ surfaces was assessed by XPS and is shown for the multilayer (Fig 2a-b) and the monolayer (Fig 2c-d).

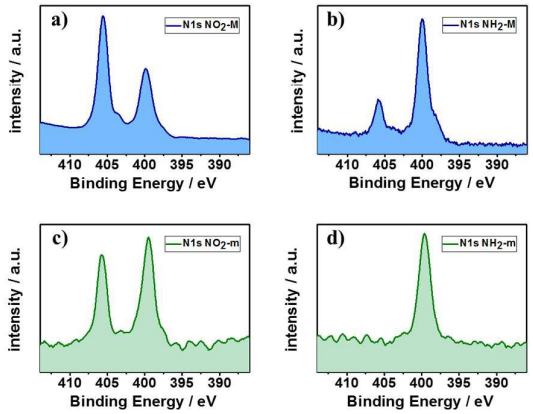

Figure 2. N1s spectra of a) NO_2-M; b) NH_2-M; c) NO_2-m and d) NH_2-m.

The N1s core level spectra for modified surfaces are characterized by two principal signals at E_b=406 eV (NO_2 groups) and E_b=400 eV (reduced nitrogen species). For NO_2-M and NO_2-m samples (Fig 2a and 2c) these two peaks are clearly noticeable. However, for NH_2-M and NH_2-m (Fig 2b and 2d) the latter appears in a higher intensity, while the signal at 406 eV diminishes dramatically (Fig 2b), and even disappears (Fig 2d). It should be noted that the presence of these two peaks in the case of NO_2-M and NO_2-m is a result of cycling the potential successively during the electrochemical film formation process. These cycles produce the reduction of a certain percentage of nitro groups (E_b=406 eV) on the surface. This peak at E_b= 400 eV can be appreciated more clearly in NO_2-m (Fig 2c), where the number of electrochemical runs for the film formation is even higher as it was commented in section 3.1. In the case of NH_2-M and NH_2-m samples, the peak at 400 eV is related to different nitrogen species such as $-NH_2$ groups and azo bridges found in the direct anchorage of the molecules on the surface or in the polyaryl structure formed.[31, 37] The disappearance of the signal associated with nitrophenyl groups in these samples (Fig 2b and d) evidences the efficiency of the reduction process to amine groups in both multilayer and monolayer films. Moreover, it has been stablished that the weak signal at around 402.6 eV detected as a small shoulder in figures 2b and d can be assigned to nitrosophenyl and hydroxylamine groups generated by partial reduction of nitro groups. Finally, it should be commented that [N1s/C1s] ratio is quite different depending on the film thickness, being 7 ± 2 % in the case of the multilayer (Fig 2a-b) and 1.5 ± 0.2 % in the case of the monolayer (Fig 2c-d) films.

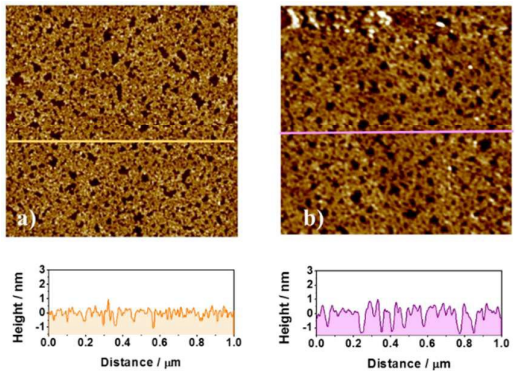

Figure 3. AFM images (1 µm x 1 µm) corresponding to (a) NO_2 -m and (b) NH_2-m. Each image incorporates a representative cross section of the surface profile.

AFM images corresponding to NO_2-M and NH_2-M are shown in Supplementary Information S1. The film thickness for the multilayer has been determined by scratching the surface with the AFM tip, obtaining a value near to 6 +/- 1.8 nm (Supplementary Information S2). It is well known that the height corresponding to a nitrophenyl group oriented perpendicularly on a flat surface is 0.8 nm,[33] i.e. our multilayer film is formed by a minimum of 8-9 layers. It is generally accepted that the growth reaction consists on the reduction of aryl diazonium ions producing an aryl radical which forms a covalent bond on the surface. A disordered multilayer film is obtained as the reaction takes place due to the continuous attack of radicals and the incorporation to the molecules anchored on the surface.[38] The origin of the interaction between aryl radical and the HOPG basal plane has been the goal of many studies. The main discussion is around the proportion on the covalently bonded molecules (grafted) regarding those which are exclusively physisorbed on the surface. Ma et al. have showed the existence of a covalent bond of the organic layer in the HOPG steps while the rest of the layer consists of physisorbed oligomers.[39] Recently, a grafting mechanism of some molecules followed by a 3D growth of the layer has been proposed.[40] In this case, the radicalary attack reaction results favored and produce the observed 3D growth inhibiting at the same time the grafting reaction on the adjacent carbon atoms and producing a sp^3/sp^2 ratio lower that that corresponding to a fully chemisorbed layer. Nevertheless, it seems clear that there is always a mixture of grafted and physisorbed molecules.

When the grafting process is made in the presence of 2 mM DPPH, evident morphological changes in the surface structure can be observed as compared with the multilayer case. By cycling the potential as it is indicated in Figure 1b the NO_2-m progressively grows. After a couple of voltammetric cycles a number of big holes mostly covers de HOPG surface. These holes become smaller as the number of electrochemical cycles increases leaving finally a homogeneously distributed monolayer on the HOPG surface (Supplementary Information S3). Figures 3a-b show the film

generated after 8 cycles by using this radical scavenger for NO_2-m and NH_2-m, respectively. It should be noted that now the film thickness is much lower, giving values around 0.8-1.3 nm. This thickness, which is consistent with the organic monolayer, confirms the efficiency of the radical scavenger to control the number of layers in the organic structure. As can be seen there are still some small holes in the film (black regions in Fig. 3a-b) that cover homogeneously the entire surface leaving some free HOPG areas. It is important to note that these regions are observed in the HOPG surface but there is not evidence of them in other substrates like pyrolyzed photoresist film (PPF).[31] These holes are around 28-40 nm in size and represent around 20-30 % of the surface. In other words, the monolayer is strictly speaking a submonolayer covering the 70-80 % of the surface area. In this case, the reduction process modifies slightly only the diameter but not the depth of the holes.

With the aim to study at the nanoscale the non-conductive behavior of the multilayer functionalized surface, C-AFM measurements of this system were made and are shown in Supplementary Information S4. The images show the very different distribution of electrical conductance between the clean HOPG surface and the deposited organic film. While the free HOPG surface shows a response which perfectly follows the applied difference potential, the organic covered surface appears totally passivated after the functionalization with aryl diazonium salts. This surface passivation has been observed before for layers formed by long chain diazonium salts.[41] By performing i-V curves in C-AFM contact mode on these covered and uncovered areas, the same conclusions can be obtained (Supplementary Information S5).

In order to check the electrochemical behavior for the multilayer and monolayer organic films, two different redox probes, namely $Fe(CN)_6^{4-}$/ $Fe(CN)_6^{3-}$ and dopamine, were used. Some interesting results regarding this point are shown in Figure 4a-b and Supplementary Information S6. Voltammograms corresponding to the electrochemical response onto free HOPG surface are included (black line) for comparison in all cases. As it can be seen when the electrode is not functionalized the response of both redox probes shows a small difference in their peak potential (ΔE_p) that implies a good electron-transfer rate.

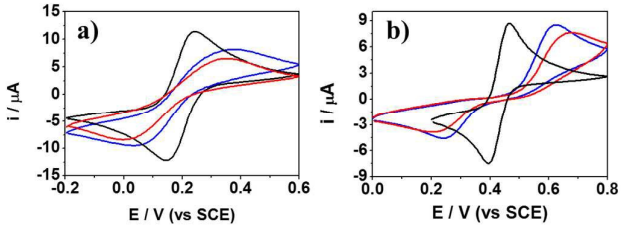

Figure 4. Cyclic voltammograms showing the electrochemical response (black: HOPG; blue: NO_2; red: NH_2) of (a) 1 mM $[Fe(CN)_6]^{4-}$ /$[Fe(CN)_6]^{3-}$ + 0.1 M KNO_3 for monolayer films and (b) 1 mM dopamine + 0.01 M H_2SO_4 for monolayer films.

McCreery and co-workers have studied the charge transfer kinetics for the passage of catechol to o-quinone on modified and unmodified carbon electrodes.[42] Their results demonstrate that it is neccesary the cathecol adsorption onto the electrode surface for fast electron transfer to occur. Thus, dopamine could be used as a good sensitive probe to test the presence of defects/pinholes on the surface due to dopamine only absorbs on free carbon surface. In the case of $Fe(CN)_6^{4-}$/ $Fe(CN)_6^{3-}$, the most commonly used redox probe in the literature, that exhibits a certain "inner-sphere" character, it has been shown to sense efficiently the electrochemical surface behavior as well.[43] Due to these reasons, both redox couples can be used to detect subtle modifications on the surface state.[44]

Two different electrochemical responses are found depending on the layer thickness. The electrochemical response changes completely for both probes in the case of the monolayers Fig 4 a-b as compared with multilayer films (Supplementary Information S6). As it is shown in Figure 4a and b, both probes show an irreversible electrochemical response on both NO_2-m and NH_2-m as compared with the corresponding one registered on clean HOPG surface (black line). Nevertheless, it is important to note that now ΔE_p is higher for dopamine than for the $Fe(CN)_6^{4-}$/ $Fe(CN)_6^{3-}$, i.e. dopamine response is more irreversible than $Fe(CN)_6^{4-}$/ $Fe(CN)_6^{3-}$ one. The reason for this is that dopamine adsorption is only permitted on the free HOPG areas of the holes shown in Figures 3 a-b while for the $Fe(CN)_6^{4-}$/ $Fe(CN)_6^{3-}$ probe the low thickness of the monolayer allows its electrochemical response to occur at the entire surface.

3.3. Electrodeposition of gold nanoparticles on the modified surfaces.

One of the principal advantage of the electrografting made on HOPG is undoubtedly that this method is one of the easiest to completely functionalize the HOPG surface. Nevertheless, electrografting process on HOPG paradoxically produce finally a useless surface from the electrochemical point of view due to the fact that the thickness of the organic film avoids any charge-transfer mechanism. This situation dramatically changes when the electrografting process is controlled to the growth of only a monolayer or submonolayer where not only the surface maintains a very good electrical conductance but, which is even better, some important improvement on the electrochemical response are obtained, for instance in the case of gold electrodeposition.

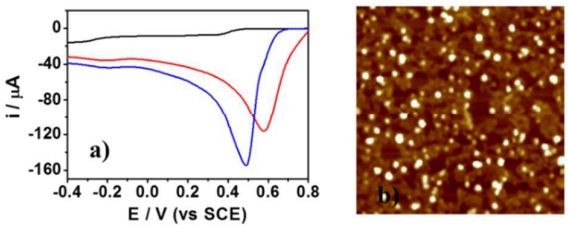

Figure 5. (a) Reduction voltammogram of 1mM $HAuCl_4$ + 0.1M KNO_3 solution (v= 0.05 V s^{-1}) on free HOPG (blue), NH_2-M (black) and NH_2-m (red). (b) Representative AFM image (0.4 µm x 0.4 µm) of gold nanoparticles (white dots) electrodeposited on the organic monolayer.

Figure 5a shows the reduction voltammogram of gold from 1 mM $HAuCl_4$ in the indicated conditions on the NH_2-M (black), NH_2-m (red) and free HOPG (blue). The electroreduction of gold on HOPG is characterized by an electroreduction peak at 0.48V followed by a small shoulder near -0.25 V before the setting of a diffusion limited current. A first principal fact is that, as expected, the electroreduction of gold on the multilayer film is strongly inhibited while on the organic monolayer film a significant higher reduction peak potential is observed. The gold reduction starts almost 0.2 V before and the electroreduction peak appears 0.1 V more positive.

A second important fact that can be clearly observed in Figure 5b is that the nucleation and growth of the electrodeposited gold nanoparticles occurs exclusively on the organic monolayer, not on the free HOPG areas. This fact is a clear consequence of the specific interaction between the nature of the organic layer and the gold ions. The usage of different functional groups to coordinate transition metal ions followed by the electrochemical reduction of these ions is a very useful technique for the nanoparticles formation.[45, 46] In this regard, it is known the nitrogen containing groups ability to coordinate certain metallic ions. For instance, Kolb and co-workers adsorbed Pd^{2+} ions on a pyridine ended self-assembled monolayer growing after that a Pd layer by electrochemical reduction.[47] When the surface of the organic layer is mostly ended in -NH_2 groups, the $AuCl_4^-$ ions are strongly fixed by these amine groups. Different interactions between amine groups and gold ions including ion pairing of $AuCl_4^-$ with amine groups, displacement of a chloride ligand by the amine or partially reduction of Au(III) to Au(I) by the amine have been described.[48] Thus, crystallization overpotential is reduced by replacing the surface free energy of the HOPG for the surface free energy of the amine terminated organic layer.

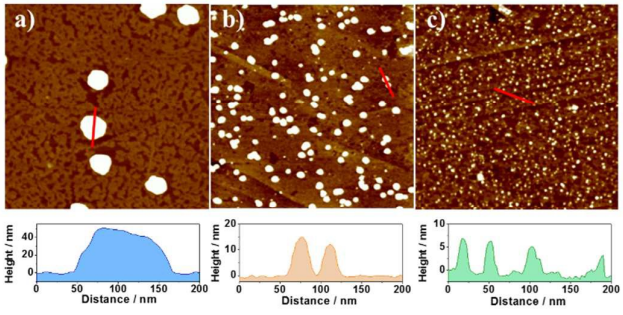

Figure 6. AFM images (1 µm x 1 µm) for different applied pulse potentials (E_d) corresponding to a charge density q= 1 mC cm^{-2}. (a) E_d=0.4 V, (b) E_d=0 V and (c) E_d=-0.4 V. Each image incorporates a cross section to observe the surface profile.

Figure 6 shows the AFM images of the gold nuclei formed as a function of the applied potential at the same electrodeposited charge density (q= 1mC cm^{-2}) for three cases. The number of nuclei and their size are highly dependent on the applied potential. Thus, at the more positive potential (E_d = 0.4 V; Fig. 6a) only a few big gold hemispherical particles grow while at lower potentials nucleation and growth of gold nanoparticles (AuNPs) homogeneously distributed on the organic monolayer is observed. In our conditions AuNPs have a radii-height ratio (r/h) very near to 1, i.e. they can be considered as hemispheres whose size strongly diminishes while their surface density grows as the applied potential becomes more negative. Supplementary Information S7 shows a table which resumes these data.

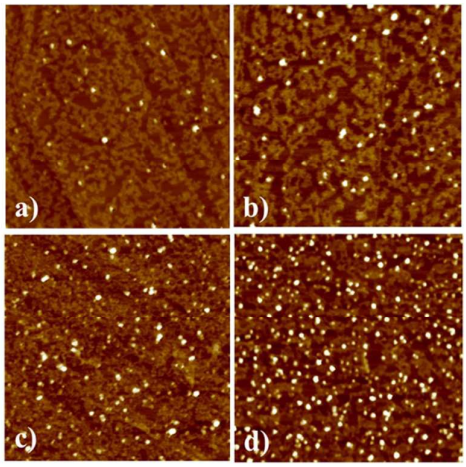

Figure 7. AFM images (0.6 µm x 0.6 µm) for a applied potential E_d= -0.4 V during (a) 0.05 s, (b) 0.5 s, (c) 5 s and (d) 20 s from a 0.1 mM $HAuCl_4$ in 0.1 M KNO_3 solution.

In Figure 7 the effect of the electrodeposition time at the most negative applied potential (E_d = -0.4V) is studied. The higher the time the larger the surface nuclei density. We have tried to fix our data to the Scharifker and Hills classical model for the nucleation and growth of metallic 3D hemispherical particles.[49,50] Supplementary Information S8 shows the results. This nucleation and growth behavior contrasts with that found on bare HOPG where nanowires growth is favoured in the steps and nanodiscs or dendrites grow on the terraces.[6,7]

The density number of formed gold nuclei fairly obeys the law:

$$N = N_0(1 - e^{-At})$$

where N_0 is the number of initially available nucleation sites at the surface and A is the steady-state nucleation rate per nucleation site. From Figure S8c our experimental data results good fixed to that law giving a value of N_0=930*10^8 particles/cm^2, i.e. near 10^{11}, and A=0.23 s^{-1}. This high number of nuclei obtained agrees quite well with previous results found in glassy carbon electrodes in the same conditions, confirming that we have transformed an inert substrate like HOPG in a reactive surface one, comparable with GC.[51]

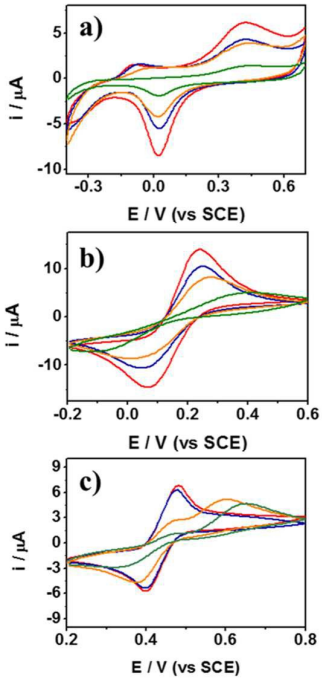

Figure 8. Cyclic voltammograms of electrodeposited AuNPs on NH_2-m for E_d= -0.4 V during the following electrodeposition times: 0.05 s (green), 0.5 s (orange), 5 s (blue) and 20 s (red). (a) in 0.1 M NaOH (v=0.1 V s^{-1}); (b) in the presence of 1 mM $[Fe(CN)_6]^{4-}$/$[Fe(CN)_6]^{3-}$ + 0.1 M KNO_3 and (c) in the presence of 1 mM dopamine + 0.01 M H_2SO_4.

Finally and in order to test the electrochemical behaviour of the organic monolayer after gold electrodeposition, $Fe(CN)_6^{4-}$/ $Fe(CN)_6^{3-}$ and dopamine electrochemical probes were tested again on the gold-modified surfaces. These results are shown in Figure 8 as a function of the increment of AuNPs electrodeposited (as it is shown in figure 7). Thus, Figure 8a shows the cyclicvoltammogram of gold in 0.1 M NaOH. As expected, the electrochemical peaks of oxidation and reduction of gold increase accordingly to the number of AuNPs. Figures 8b and 8c show the results for $Fe(CN)_6^{4-}$/ $Fe(CN)_6^{3-}$ and dopamine, respectively. The presence of AuNPs strongly adsorbed on top of the NH_2-m accounts for a noticeable increase in the electron transfer kinetics in comparison to that exhibited by the NH_2-m electrode, Figure 4 a-b. Over the last few years significant contributions have addressed this issue concluding that the electron transfer between the underlying electrode and the AuNPs assembled on top of the organic layer is by far easier than the electron transfer between the electrode and dilute redox probes in solution.[52, 53] In this context, the electrochemical response vs. both redox probes is more reversible as the number of AuNPs increases. These results are in very good agreement with those shown by Gooding and co-workers[54] where the growing number of assembled AuNPs was accompanied by a decrease in the ΔE_p (Supplementary Information S9) and an increase in the peak current. Interestingly, in the case of dopamine when the amount of AuNPs is low (green and orange lines) the cyclovoltammogram contains two cathodic and two anodic peaks, more clearly seen in the oxidation potential scan. As the number of AuNPs grows the first oxidation peak increases accordingly while the second one appears at lower potential. The final voltammogram only contains a reversible couple of peaks. Taking into account that dopamine electrochemical response is negligible on the organic film, our results indicate that we are observing how the dopamine oxidation peak on AuNPs grows (the first and more reversible one) respect to that on the clean HOPG areas. When the AuNPs is high enough (red line) the contribution to the faradaic current on the AuNPs is the principal one detected. It should be noted that this result does not depend on the applied potential, i.e. it is obtained regardless of the AuNPs size. In resume, HOPG surface modification, as indicated in the present work, opens a wide field of potential electrochemical applications.

Conclusions

The novelty of our paper is to describe the conditions for a controlled modification (at the monolayer level) of a well-defined, relatively cheap, and chemically inert substrate which also allows easy characterization at nanoscale level due to the atomically smooth surface.

The electrografting process by using DPPH allows to grow an organic monolayer film on HOPG surface transforming this chemically inert surface into highly reactive one with potential electrochemical applications. In our experimental conditions the monolayer covers the 70-80% of the HOPG surface. Thus, it is actually a submonolayer and its thickness corresponds to that expected for a nitrophenyl molecule oriented perpendicularly to the surface.

This monolayer shows an important electrical conductivity that allows its use for electrochemical applications. Thus, on the monolayer surface charge-transfer reactions can take place easily.

In our conditions gold electrodeposition results importantly favored on the organic monolayer film while it does not take place on the free HOPG areas. This result offers the possibility of technological applications by using patterned graphite or graphene surfaces. The nucleation and growth mechanism is a progressive one forming 3D hemispherical AuNPs homogeneously distributed only onto the organic surface and of sizes that can be well controlled by the electrodeposition applied potential.

The redox behavior of $Fe(CN)_6^{4-}$/ $Fe(CN)_6^{3-}$ and dopamine probes have been tested on the organic monolayers and on the AuNPs-modified surfaces. Both probes show a voltammogram sensitive to the number of AuNPs decreasing ΔE_p as the number of AuNPs increases. The presence of AuNPs strongly adsorbed on top of the NH_2-m accounts for a noticeable increase in the electron transfer kinetics in comparison to that exhibited by the NH_2-m electrode.

Acknowledgements

This work was founded by MINECO Spain under project number CTQ2011-24784. M.C.R.G. thanks to Spanish MEC for a FPU research grant (FPU2014/00886). A.G.O acknowledges

Cajasiete for a SEGAI grant. Authors acknowledge SEGAI of the ULL for the XPS measurements.

Notes and references

1 E. Budevski, G. Staikov, W. Lorenz and K. Keusler, *Electrochemical phase formation and growth*, Wiley-VCH, 1997.

2 B. R. Scharifker and J. Mostany, *Dev. in Electrochem. : Sci. Inspired by Martin Fleischmann,* 2014, 65-75.

3 U. S. Mohanty, *J. Appl. Electrochem.,* 2011, **41**, 257-270.

4 A. J. Bard, *J. Am. Chem. Soc.,* 2010, **132**, 7559-7567.

5 S. E. F. Kleijn, S. C. S. Lai, M. T. M. Koper and P. R. Unwin, *Angew. Chem. Int. Ed.,* 2014, **53**, 3558-3586.

6 H. Martín, P. Carro, A. Hernández Creus, S. González, R. C. Salvarezza and A. J. Arvia, *Langmuir,* 1997, **13**, 100-110.

7 H. Martín, P. Carro, A. Hernández Creus, S. González, G. Andreasen, R. C. Salvarezza and A. J. Arvia, *Langmuir,* 2000, **16**, 2915-2923.

8 Y. Gimeno, A. Hernández Creus, S. González, R. C. Salvarezza and A. J. Arvia, *Chem. Mater.,* 2001, **13**, 1857-1864.

9 Y. Gimeno, A. Hernández Creus, P. Carro, S. González, R. C. Salvarezza and A. J. Arvia, *J Phys Chem B,* 2002, **106**, 4232-4244.

10 C. J. Boxley, H. S. White, T. E. Lister and P. J. Pinhero, *J Phys Chem B,* 2003, **107**, 451-458.

11 T. Brülle and U. Stimming, *J Electroanal Chem,* 2009, **636**, 10-17.

12 M. Bayati, J. M. Abad, R. J. Nichols and D. J. Schiffrin, *J. Phys. Chem. C,* 2010, **114**, 18439-18448.

13 S. C. S. Lai, R. A. Lazenby, P. M. Kirkman and P. R. Unwin, *Chem. Sci.,* 2015, **6**, 1126-1138.

14 Y. Kim, S. C. S. Lai, K. McKelvey, G. Zhang, D. Perry, T. S. Miller and P. R. Unwin, *J. Phys. Chem. C,* 2015, **119**, 17389-17397.

15 C. E. Banks and R. G. Compton, *Analyst,* 2006, **131**, 15-21.

16 P. Allongue, M. Delamar, B. Desbat, O. Fagebaume, R. Hitmi, J. Pinson and J. Savéant, *J. Am. Chem. Soc.,* 1997, **119**, 201-207.

17 D. Bélanger and J. Pinson, *Chem. Soc. Rev.,* 2011, **40**, 3995-4048.

18 J. J. Gooding, *Electroanalysis,* 2008, **20**, 573-582.

19 S. Mahouche-Chergui, S. Gam-Derouich, C. Mangeney and M. M. Chehimi, *Chem. Soc. Rev.,* 2011, **40**, 4143-4166.

20 S. Y. Sayed, A. Bayat, M. Kondratenko, Y. Leroux, P. Hapiot and R. L. McCreery, *J. Am. Chem. Soc.,* 2013, **135**, 12972-12975.

21 H. Gehan, L. Fillaud, N. Felidj, J. Aubard, P. Lang, M. M. Chehimi and C. Mangeney, *Langmuir,* 2010, **26**, 3975-3980.

22 M. Bayati and D. J. Schiffrin, *J. Phys. Chem. C,* 2013, **117**, 22746-22755.

23 F. Mirkhalaf, K. Tammeveski and D. J. Schiffrin, *Phys. Chem. Chem. Phys.,* 2009, **11**, 3463-3471.

24 D. J. Guo and H. L. Li, *Carbon,* 2005, **43**, 1259-1264.

25 M. Bayati, J. M. Abad, C. A. Bridges, M. J. Rosseinsky and D. J. Schiffrin, *J Electroanal Chem,* 2008, **623**, 19-28.

26 G. Zeb, P. Gaskell, X. T. Le, X. Xiao, T. Szkopek and M. Cerruti, *Langmuir,* 2012, **28**, 13042-13050.

27 J. Pinson and F. Podvorica, *Chem. Soc. Rev.,* 2005, **34**, 429-439.

28 O. Fontaine, J. Ghilane, P. Martin, J. Lacroix and H. Randriamahazaka, *Langmuir,* 2010, **26**, 18542-18549.

29 Y. R. Leroux, H. Fei, J. Noël, C. Roux and P. Hapiot, *J. Am. Chem. Soc.,* 2010, **132**, 14039-14041.

30 T. Menanteau, E. Levillain and T. Breton, *Chem. Mater.,* 2013, **25**, 2905-2909.

31 T. Menanteau, E. Levillain, A. J. Downard and T. Breton, *Phys. Chem. Chem. Phys.,* 2015, **17**, 13137-13142.

32 M. Delamar, R. Hitmi, J. Pinson and J. M. Savéant, *J. Am. Chem. Soc.,* 1992, **114**, 5883-5884.

33 P. A. Brooksby and A. J. Downard, *Langmuir,* 2004, **20**, 5038-5045.

34 M. Kullapere, F. Mirkhalaf and K. Tammeveski, *Electrochim. Acta,* 2010, **56**, 166-173.

35 B. Ortiz, C. Saby, G. Y. Champagne and D. Bélanger, *J Electroanal Chem,* 1998, **455**, 75-81.

36 C. Saby, B. Ortiz, G. Y. Champagne and D. Bélanger, *Langmuir,* 1997, **13**, 6805-6813.

37 A. Adenier, E. Cabet-Deliry, A. Chaussé, S. Griveau, F. Mercier, J. Pinson and C. Vautrin-Ul, *Chem. Mater.,* 2005, **17**, 491-501.

38 P. Doppelt, G. Hallais, J. Pinson, F. Podvorica and S. Verneyre, *Chem. Mater.,* 2007, **19**, 4570-4575.

39 H. Ma, L. Lee, P. A. Brooksby, S. A. Brown, S. J. Fraser, K. C. Gordon, Y. R. Leroux, P. Hapiot and A. J. Downard, *J. Phys. Chem. C,* 2014, **118**, 5820-5826.

40 J. Greenwood, T. H. Phan, Y. Fujita, Z. Li, O. Ivasenko, W. Vanderlinden, H. Van Gorp, W. Frederickx, G. Lu, K. Tahara, Y. Tobe, H. Uji-I, S. F. L. Mertens and S. De Feyter, *ACS Nano,* 2015, **9**, 5520-5535.

41 S. Lin, C. Lin, J. Jhang and W. Hung, *J. Phys. Chem. C,* 2012, **116**, 17048-17054.

42 S. H. DuVall and R. L. McCreery, *Anal. Chem.,* 1999, **71**, 4594-4602.

43 R. L. McCreery, *Chem. Rev.,* 2008, **108**, 2646-2687.

44 S. Lhenry, Y. R. Leroux and P. Hapiot, *Anal. Chem.,* 2012, **84**, 7518-7524.

45 D. Qu and K. Uosaki, *J Phys Chem B,* 2006, **110**, 17570-17577.

46 C. Silien, D. Lahaye, M. Caffio, R. Schaub, N. R. Champness and M. Buck, *Langmuir,* 2011, **27**, 2567-2574.

47 M. Manolova, V. Ivanova, D. M. Kolb, H. Boyen, P. Ziemann, M. Büttner, A. Romanyuk and P. Oelhafen, *Surf. Sci.,* 2005, **590**, 146-153.

48 C. J. Clukay, C. N. Grabill, M. A. Hettinger, A. Dutta, D. J. Freppon, A. Robledo, H. Heinrich, A. Bhattacharya and S. M. Kuebler, *Appl. Surf. Sci.,* 2014, **292**, 128-136.

49 B. Scharifker and G. Hills, *Electrochim. Acta,* 1983, **28**, 879-889.

50 M. E. Hyde and R. G. Compton, *J Electroanal Chem,* 2003, **549**, 1-12.

51 G. Gotti, K. Fajerwerg, D. Evrard and P. Gros, *Electrochim. Acta,* 2014, **128**, 412-419.

52 J. Chazalviel and P. Allongue, *J. Am. Chem. Soc.,* 2011, **133**, 762-764.

53 A. Barfidokht, S. Ciampi, E. Luais, N. Darwish and J. J. Gooding, *ChemPhysChem,* 2013, **14**, 2190-2197.

54 A. Barfidokht, S. Ciampi, E. Luais, N. Darwish and J. J. Gooding, *Anal. Chem.,* 2013, **85**, 1073-1080.